CHAPTER IV
RESULTS AND DISCUSSION

4.1 Chemical compositions of silica gel waste

The chemical components of silica gel waste in the form of stable oxides are shown in Table 3. The major component was SiO_2, along with small amounts of other inorganic oxides, including Na_2O, MgO, TiO_2, CaO, and Fe_2O_3. Furthermore, the amorphous-phase silica obtained could be advantageous for zeolite synthesis, as it dissolves easily in NaOH solution to yield sodium silicate (Na_2SiO_3) (Keawkumay et al., 2024).

Table 3 Elemental composition of silica gel waste determined by XRF analysis.

Sample	Component (wt%)					
	SiO_2	Na_2O	MgO	TiO_2	CaO	Fe_2O_3
Silica gel waste	95.96	1.86	1.36	0.33	0.23	0.27

4.2 Characterization of synthesized zeolites

The SEM images in Figure 7 illustrate the morphologies of six zeolite samples, including synthesized and commercial forms of Zeolite A, X, and Y, all synthesized using silica gel waste as a silica source. Zeolite A, shown in images (a) and (d), exhibits a well-defined cubic morphology with smooth surfaces and sharp edges, indicative of high crystallinity. The synthesized zeolite A (a) consists of smaller, uniform cubic crystals with a size of 0.46 ± 0.041 μm, whereas the commercial zeolite A (d) features larger, more distinct cubic structures with a size of 2.0 ± 0.13 μm.

Zeolite X, presented in images (b) and (e), exhibits a polycrystalline structure with intergrown crystallites forming aggregated particles. The synthesized zeolite X (b) has a rough and irregular morphology, with a shape resembling a Takraw ball, where the crystallites appear interwoven and interconnected, with a size of 1.1 ± 0.10 μm.

In contrast, the commercial zeolite X (e) consists of more well-defined and larger crystals, some showing partially truncated octahedral shapes, with a size of 2.2 ± 0.24 μm.

Zeolite Y, shown in images (c) and (f), has a highly porous and loosely packed morphology. The synthesized zeolite Y (c) consists of fine, irregularly aggregated particles with a size of 0.14 ± 0.019 μm, whereas the commercial zeolite Y (f) displays larger, fragmented crystals with a rough and textured surface, measuring 0.62 ± 0.041 μm. These differences in morphology and particle size between the synthesized and commercial samples indicate variations in crystallization conditions, degree of crystallinity, and structural purity.

XRD patterns of synthesized and commercial zeolite A, X, Y are shown in Figure 8. Main peaks of zeolite A, X, Y were similar to those of the commercial zeolites indicating zeolites is pure phase. Then, XRD patterns of pure-phase zeolite NaX on the diffraction peaks at 2θ ~ 7° are impurity phases. Then, the XRD pattern of synthesized zeolite Y represents the low peak intensity, which indicates low crystallinity compared with commercial zeolite Y. Low crystallinity suggests incomplete growth or poor ordering of the crystalline. The results indicated that silica gel waste can be used as a precursor in the synthesis of phase-pure zeolite A, X, Y.

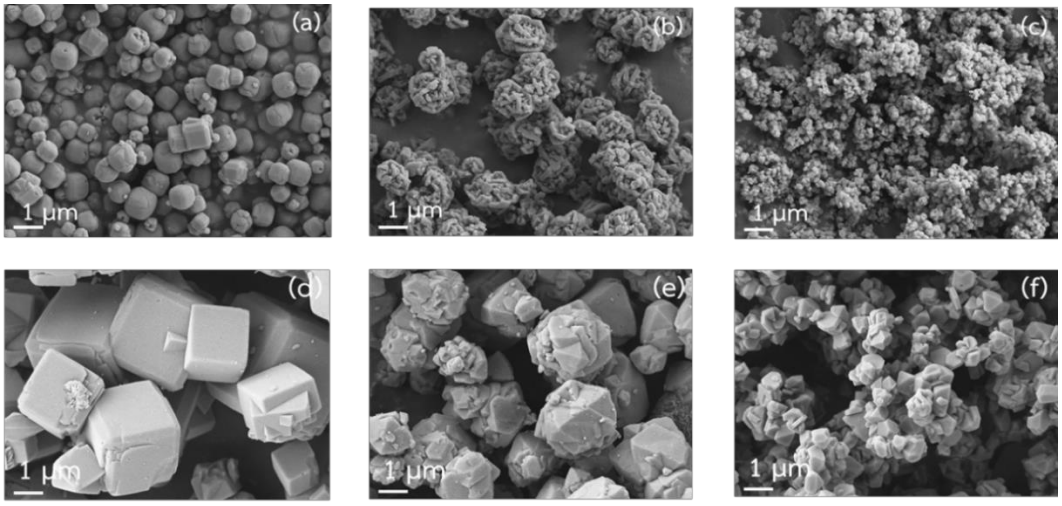

Figure 7 SEM image of synthesized zeolite A (a), synthesized zeolite X (b), synthesized zeolite Y (c), commercial A (d), commercial X (e), and commercial Y (f) by using silica gel waste as silica source with a magnification of 10 KX.

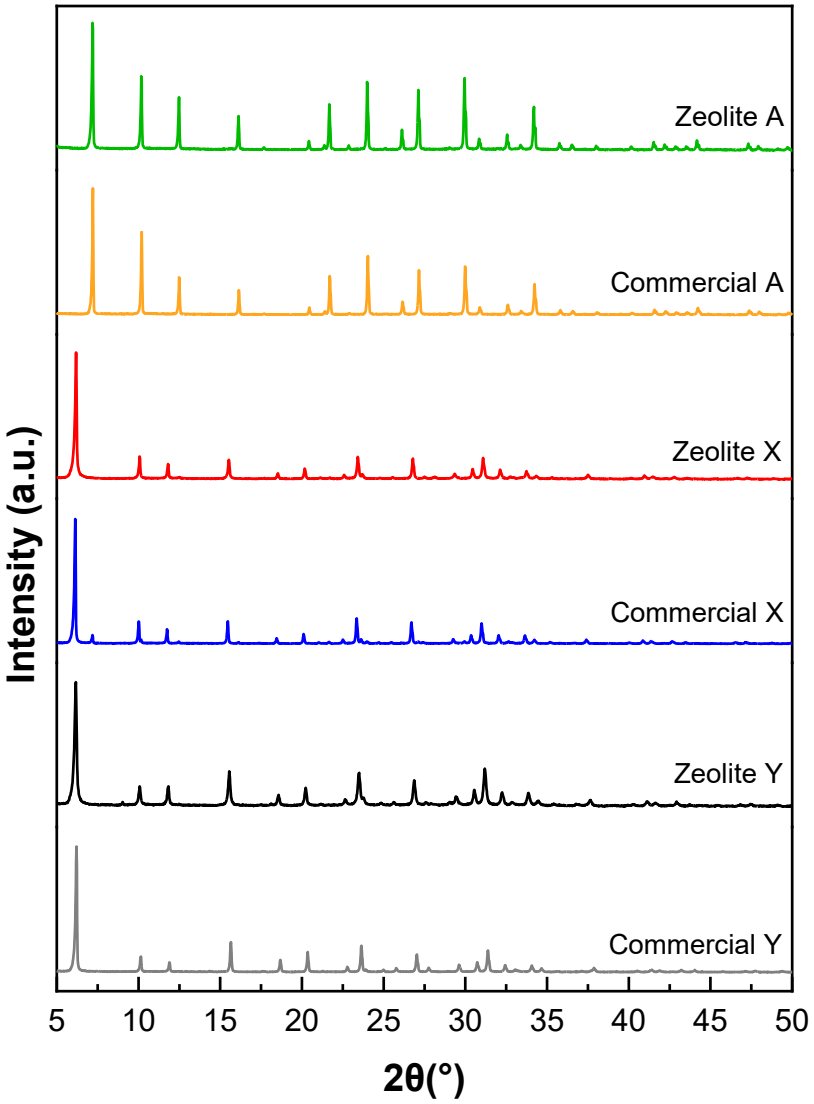

Figure 8 XRD pattern of synthesized and commercial zeolites.

FTIR spectra were recorded in the 400–4000 cm^{-1} range to identify the vibrational functional group vibrations in the zeolite structure. The spectra of the synthesized zeolite and commercial NaA, NaX, and NaY are presented in Figure 9. The bands corresponding to the internal deformation vibration modes of T-O-T bridges (where T = Si, Al) and the internal T-O symmetric stretching vibrations are only slightly affected by the Si/Al ratio. Transmittance peaks were observed at 465 and 663 cm^{-1} for zeolite NaA, and at 453 and 669 cm^{-1} for zeolite NaX, respectively. The band corresponding to the asymmetric external vibration of the double four-rings in the zeolite framework is more sensitive to the Si/Al ratio, appearing at 550 cm^{-1} for zeolite

NaA and at 561 cm^{-1} for zeolite NaX. The T–O–T vibration band gives a peak at 748 cm^{-1}, observed only for zeolite NaX. The internal T-O asymmetric stretching vibration produces peaks at 987 cm^{-1} for zeolite NaA and at 976 cm^{-1} for zeolite NaX. In both spectra, bands around 1640 and 3370 cm^{-1} are observed, corresponding to the presence of H_2O and hydroxyl groups, respectively. These FTIR bands are consistent with those previously reported for zeolite A and zeolite X (Keawkumay et al., 2024; Tsitsishvili, 2019).

The synthesized zeolite NaY exhibits six prominent peaks characteristic of the zeolite NaY framework. The band at 566 cm^{-1} corresponds to the double-ring vibration characteristic of the FAU zeolite framework. The band at 993 cm^{-1} is assigned to asymmetric and symmetric stretching vibrations of Si–O–Si, Si–O–Al, and O–Al–OH within the internal TO_4 structure (T = Si, Al). The bands at 1146 and 770 cm^{-1} are attributed to the asymmetric and symmetric stretching vibrations of the external TO_4 structure (T = Si, Al), respectively. The band at 1390 cm^{-1} is attributed to the double-ring external linkage associated with the FAU structure. The band at 3420 cm^{-1} corresponds to Si–OH, Si–OH–Al, and OH hydroxyl groups (Mekki et al., 2020). The characteristic bands of the zeolite NaY sample are weaker compared to those of the other materials, indicating a decrease in crystallinity, which aligns with the XRD analysis results. Furthermore, the FTIR patterns of the synthesized zeolite samples closely resemble those of the commercial zeolites. This result suggests that the zeolite synthesized from silica gel waste has a zeolite phase.

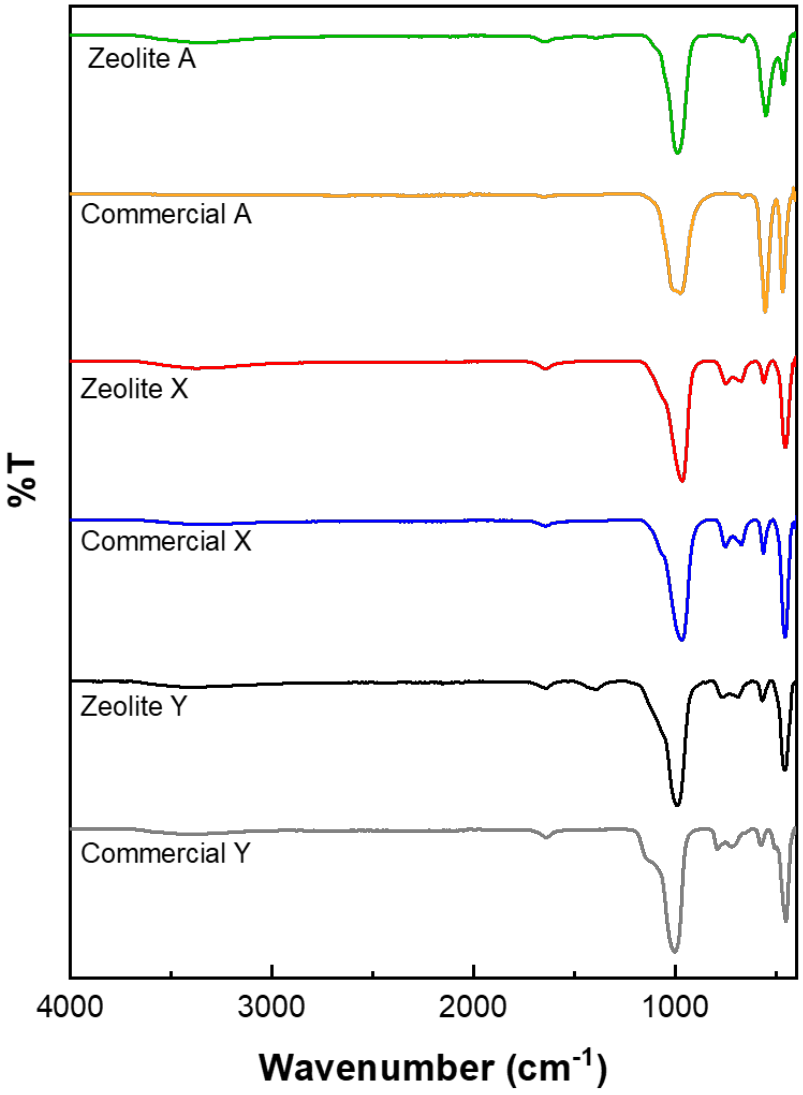

Figure 9 FTIR spectra synthesized and commercial zeolites.

Figure 10 shows the SEM-EDS mapping of NaA, NaX, and NaY zeolites, illustrating the elemental distribution of Al, Si, O, and Na across the zeolite particles. The Si/Al ratios are presented in Table 4.

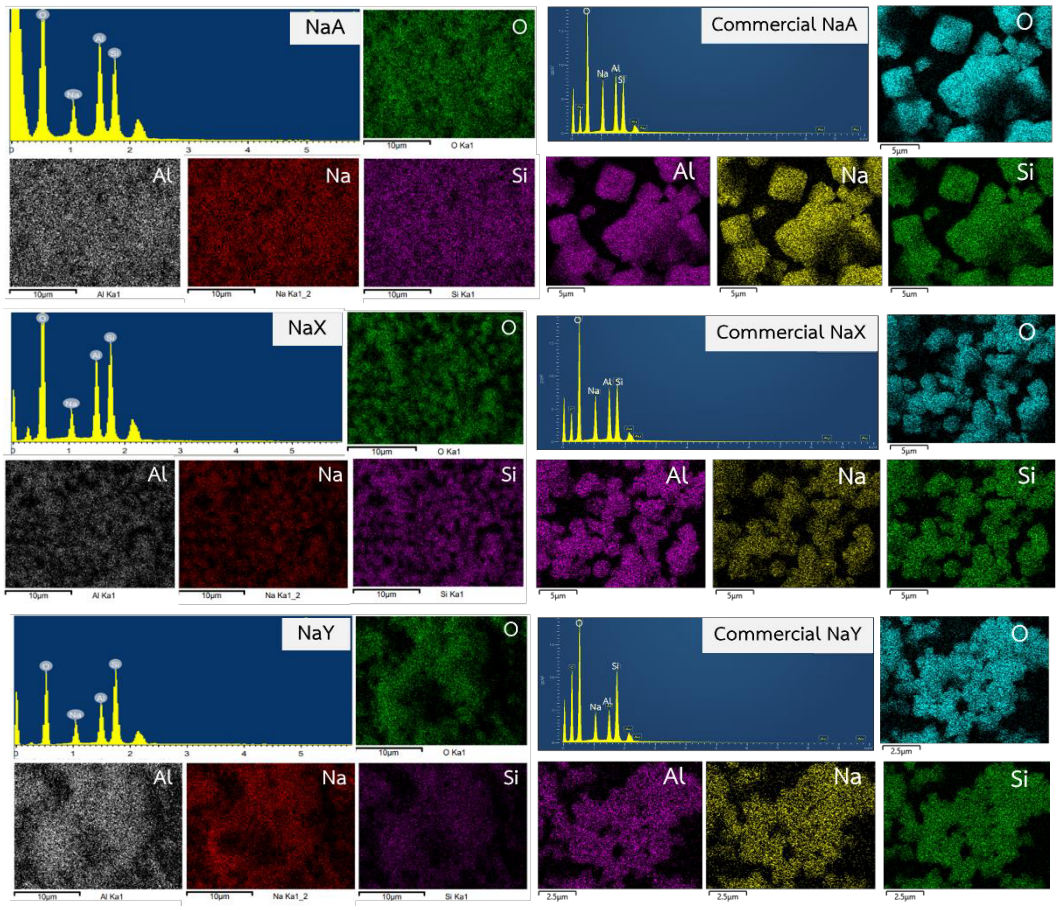

Figure 10 SEM-EDS mapping of synthesized and commercial NaA, NaX and NaY.

Table 4 Synthesis gel composition and Si/Al ratio of the zeolite products.

Sample	Synthesis gel composition			Si/Al ratio[a]	Si/Al ratio[b]
	$NaOH/SiO_2$	SiO_2/Al_2O_3	H_2O/SiO_2		
Zeolite A	10	0.5	145	1.01±0.010	1.17±0.024
Zeolite X	4	4	22	1.46±0.033	1.67±0.023
Zeolite Y	0.462	10	18	2.11±0.155	2.25±0.007

[a]SEM-EDS

[b]ED-XRF

Figure 11 displays the N_2 adsorption–desorption isotherms of all zeolites. Both the synthesized and commercial zeolites exhibit Type I(a) isotherms, characteristic of microporous materials with predominantly narrow micropores (< ~1 nm). The steep

uptake at low P/P_0 reflects micropore filling due to strong adsorbent-adsorptive interactions, with adsorption capacity primarily determined by micropore volume rather than surface area. Additionally, the presence of H4 hysteresis at $P/P_0 > 0.4$ indicates the coexistence of mesopores (2–50 nm) alongside micropores, while the pronounced uptake at low P/P_0 corresponds to micropore filling (Thommes et al., 2015).

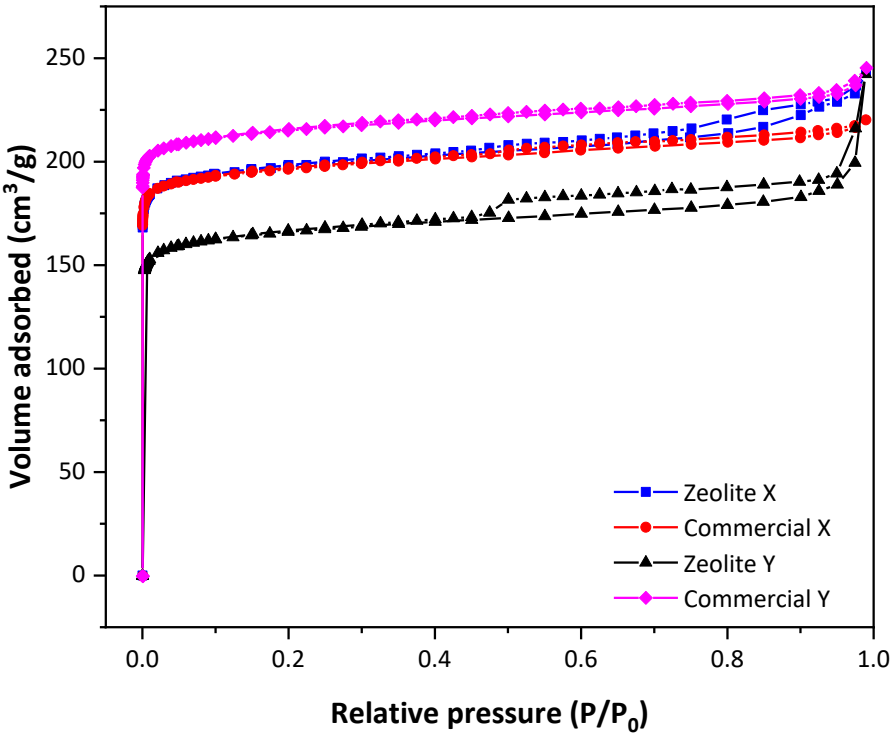

Figure 11 N_2 adsorption–desorption isotherms of zeolite NaA, zeolite NaX and zeolite NaY using silica gel waste as silica source.

Table 5 summarizes the BET surface area, external surface area, micropore surface area, and micropore volume of the synthesized and commercial zeolites. The surface area of the synthesized NaX was comparable to that of the commercial NaX, while the synthesized NaY exhibited a significantly lower surface area than its commercial counterpart. This difference is attributed to the lower crystallinity of the synthesized NaY, which leads to structural defects and a non-uniform pore distribution. These defects likely result in gaps or voids between particles, forming

interparticle voids or mesopores, ultimately reducing the overall surface area (Yates, 1968).

Table 5 Surface area of Synthesized Zeolites Determined from N_2 Adsorption–Desorption Isotherms.

Samples	Surface area[a] (m^2/g)	External surface area[b] (m^2/g)	Micropore surface area[b] (m^2/g)	Micropore volume[b] (cm^3/g)
Zeolite X	800	58	744	0.27
Commercial X	800	41	759	0.28
Zeolite Y	669	54	615	0.23
Commercial Y	876	42	835	0.30

[a]BET method

[b]*t*-plot method

Figure 12 presents the CO_2-TPD profiles of synthesized and commercial zeolites, showing two desorption temperature regions: 150-300 °C, corresponding to weak and medium basic sites, and above 300 °C, indicating strong basic sites. The corresponding basicity of each sample is summarized in Table 6. CO_2-TPD was used to evaluate the strength of basic sites in zeolites for CO_2 adsorption. The basicity follows the order: Commercial A > Zeolite A > Commercial X > Zeolite X > Commercial Y > Zeolite Y. The variation in basic site strength correlates with the Si/Al ratio and pore sizes of zeolites. A lower Si/Al ratio in zeolite NaA results in a higher incorporation of aluminum atoms into the framework, increasing the density of negatively charged sites AlO_4^-, which enhanced basicity. In contrast, the larger pores of NaX and NaY facilitate easier diffusion CO_2 molecules, leading to weaker interactions with the zeolite surface. As a result, CO_2 desorption requires less energy, manifesting as lower desorption temperatures and reduced basic site strength.

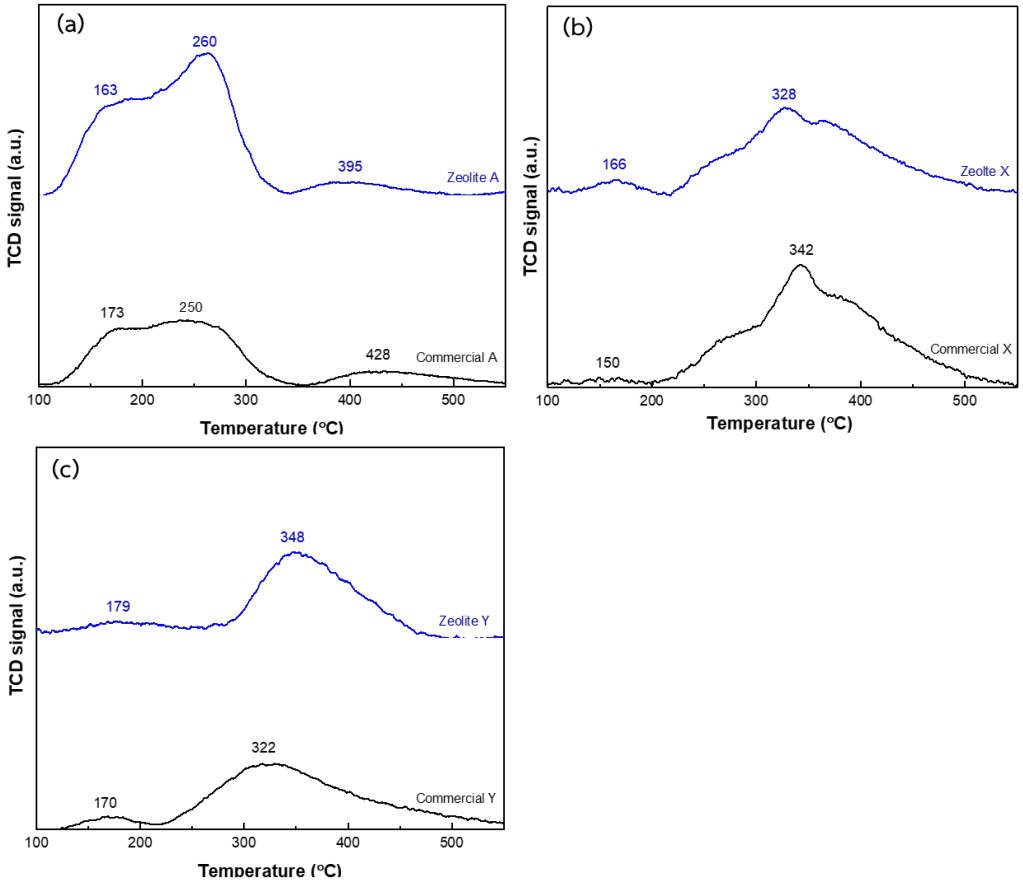

Figure 12 CO_2-TPD profiles of synthesized and commercial NaA (a), synthesized and commercial NaX (b) and synthesized and commercial NaY (c).

Table 6 Basicity of synthesized and commercial zeolites.

Samples	Basicity (mmol g^{-1})
Zeolite A	0.135
Commercial A	0.139
Zeolite X	0.052
Commercial X	0.068
Zeolite Y	0.037
Commercial Y	0.039

4.3 CO_2 adsorption capacity

Figure 13 displays the CO_2 adsorption isotherms of NaA, NaX, NaY, and their commercial counterparts. According to the IUPAC classification, all isotherms are Type

I, indicating monolayer adsorption. The isotherms exhibit a sharp uptake at low pressure due to the abundance of adsorption sites, followed by a gradual decline in adsorption rate before stabilizing at higher pressures. The adsorption behavior remains stable near 1 bar.

The primary interactions between zeolites and CO_2 molecules are predominantly electrostatic. Zeolites adsorb CO_2 through strong quadrupolar interactions between the adsorbate molecules and the electric field generated by the charge-balancing cations within the zeolite cavity. The type and spatial distribution of these cations (e.g., Na^+) influence the strength and uniformity of the electric field, thereby affecting adsorption behavior. At low pressures, CO_2 uptake increases significantly due to the availability of accessible cations in the zeolite cavities. However, at higher relative pressures, once all cations are occupied, the adsorption curve plateaus, indicating a nearly constant adsorption capacity (Bonenfant et al., 2008; Keawkumay et al., 2024; Siriwardane et al., 2005).

The CO_2 adsorption capacity followed the order: zeolite NaX > commercial NaX > commercial NaY > zeolite NaY > Commercial NaA > zeolite NaA. This trend strongly correlates with the total number of basic sites (Table 6) and the structural properties of the zeolites. Silicoaluminate zeolites also contain Lewis base sites, which originate from oxygen atoms adjacent to aluminum. The zeolite framework consists of tetrahedral TO_4 units (T = Si or Al) interconnected through shared oxygen atoms, generating a net negative charge. This charge is balanced by sodium ions (Na^+) (Salehi and Anbia, 2017). Both a net negative charge and the presence of Na^+ serve as active sites for CO_2 adsorption.

Zeolites with lower Si/Al ratios have a higher aluminum content, resulting in an increased number of extra-framework cations and basic sites. These active sites can interact with the acidic CO_2 molecule, leading to zeolites with lower Si/Al ratios exhibiting greater adsorption capacity and selectivity for CO_2 (Abdullahi et al., 2017). Thus, from these results, zeolite NaX shows higher adsorption capacity than the zeolite NaY (5.84 vs. 4.39 mmol g^{-1} in Table 7).

The lower CO_2 adsorption capacity of synthesized zeolite A compared to zeolite X is attributed to differences in their structural properties. Zeolite X has larger

pores (~7.4 Å) than zeolite A (~4.1 Å), allowing faster CO_2 diffusion through the pores and better access to adsorption sites, thereby enhancing adsorption capacity. In contrast, the smaller, more restrictive pores of zeolite A hinder CO_2 diffusion, limiting access to internal adsorption sites and reducing its adsorption capacity.

The synthesized NaY zeolite exhibited lower CO_2 adsorption capacity than commercial NaY, primarily due to differences in crystallinity. Since CO_2 adsorption depends on crystallinity, the reduced surface area and pore volume of synthesized NaY, resulting from lower crystallinity, led to decreased adsorption (Table 5). Conversely, the synthesized NaX samples demonstrated higher adsorption capacity than their commercial counterparts, likely due to the presence of impurity phases in commercial NaX, which negatively affect adsorption performance.

These findings confirm that zeolites synthesized from silica gel waste are effective CO_2 adsorbents due to their high adsorption capacity and straightforward synthesis process. Moreover, utilizing silica gel waste as a silica source presents a cost-effective and environmentally sustainable approach with significant potential for scalable production.

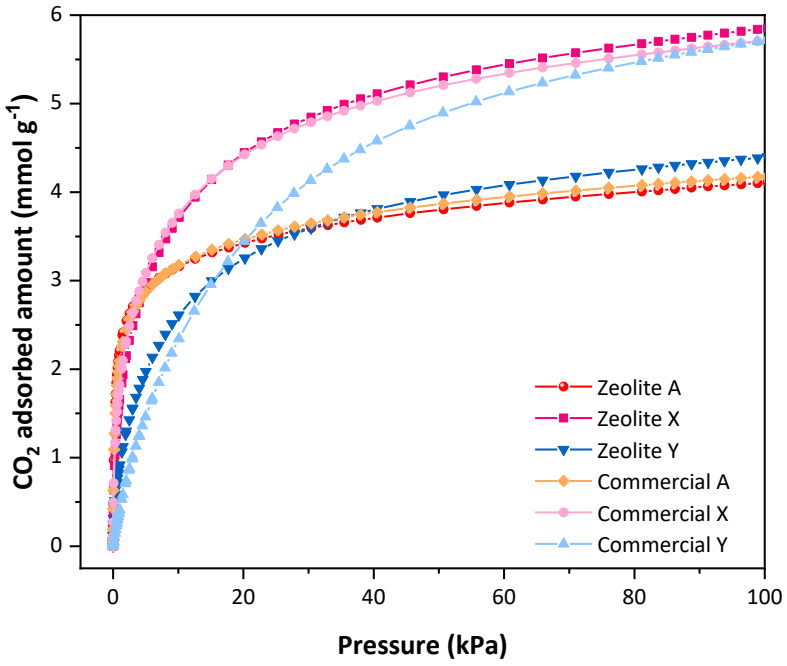

Figure 13 CO_2 adsorption isotherms of synthesized zeolites and commercial zeolites performed at 25 °C and the pressure range of 0–100 kPa.

Table 7 CO_2 adsorption capacity from synthesized and commercial zeolites.

Sample	CO_2 adsorption capacity	
	(mg g^{-1})	(mmol g^{-1})
Zeolite NaA	180	4.10
Zeolite NaX	257	5.84
Zeolite NaY	193	4.39
Commercial NaA	183	4.17
Commercial NaX	251	5.70
Commercial NaY	251	5.70

4.4 CO_2 adsorption isotherm

Figure 14 presents the CO_2 adsorption isotherm fitting with Langmuir, Freundlich, Langmuir-Freundlich, and Toth models. The correlation coefficient (R^2) values from each model from all samples are summarized in Table 8. The results indicate that CO_2 adsorption in both synthesized and commercial zeolite NaA fits well with the Toth isotherm, achieving an R^2 value greater than 0.999, better than Langmuir, Freundlich, and Langmuir-Freundlich models.

For synthesized and commercial NaX and NaY zeolites, the Sips adsorption model provided the best fit for CO_2 adsorption. A higher R^2 value signifies greater applicability and reliability of the corresponding model. These results are in good agreement with previous studies in the literature (Cui et al., 2023; Keawkumay et al., 2024; Zouaoui et al., 2021).

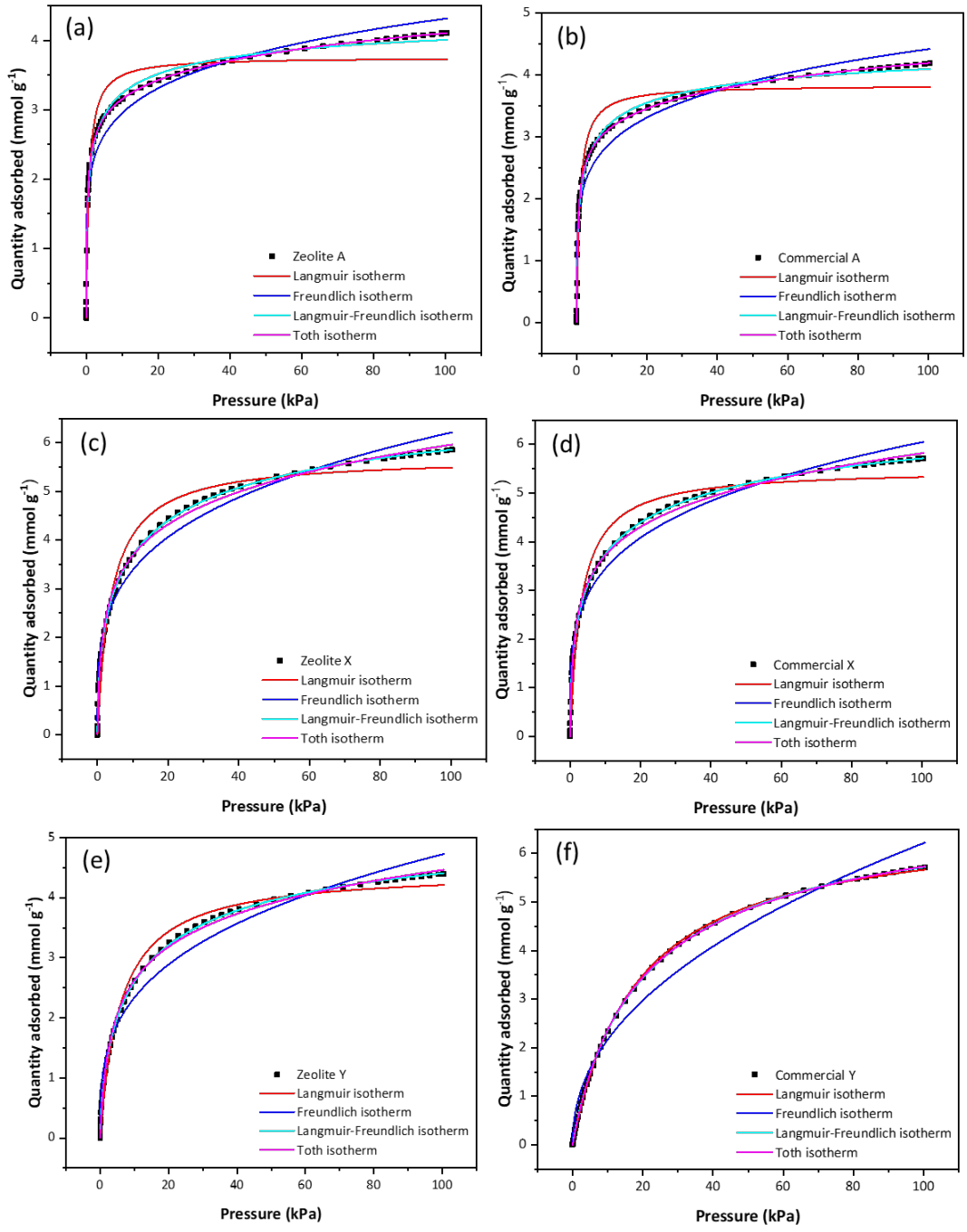

Figure 14 CO_2 adsorption isotherms of NaA (a), Commercial NaA (b), NaX (c), Commercial NaX (d), NaY (e) and commercial NaY (f) fitted with Langmuir, Freundlich, Langmuir-Freundlich and Toth models.

Table 8 Correlation coefficient (R^2) values from CO_2 adsorption isotherm of commercial and synthesized zeolites.

Samples	Correlation coefficients (R^2)			
	Langmuir	Freundlich	Langmuir-Freundlich	Toth
Zeolite NaA	0.95904	0.95622	0.99639	0.99910
Zeolite NaX	0.97434	0.98308	0.99984	0.99749
Zeolite NaY	0.98792	0.97886	0.99962	0.99747
Commercial NaA	0.96043	0.95973	0.99748	0.99952
Commercial NaX	0.96879	0.98259	0.99982	0.99762
Commercial NaY	0.99952	0.97746	0.99997	0.99984